Spatial inhomogeneity and temporal dynamics of a 2D electron gas in interaction with a 2D adatom gas

Fabien Cheynis, Stefano Curiotto, Frédéric Leroy, Pierre Müller

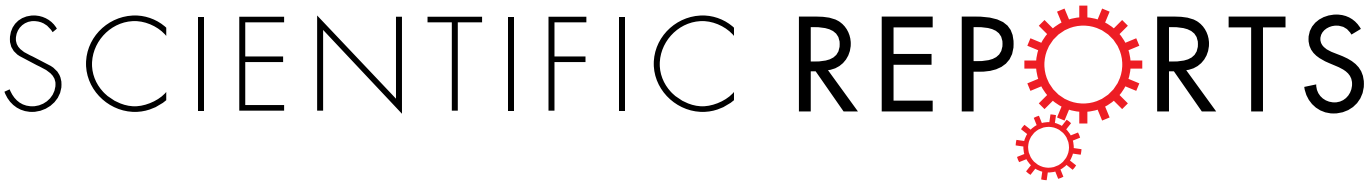

OPEN

Spatial inhomogeneity and temporal dynamics of a 2D electron gas in interaction with a 2D adatom gas

Received: 4 May 2017
Accepted: 7 August 2017
Published online: 06 September 2017

F. Cheynis, S. Curiotto, F. Leroy & P. Müller

Fundamental interest for 2D electron gas (2DEG) systems has been recently renewed with the advent of 2D materials and their potential high-impact applications in optoelectronics. Here, we investigate a 2DEG created by the electron transfer from a Ag adatom gas deposited on a Si(111) $\sqrt{3} \times \sqrt{3}$-Ag surface to an electronic surface state. Using low-energy electron microscopy (LEEM), we measure the Ag adatom gas concentration and the 2DEG-induced charge transfer. We demonstrate a linear dependence of the surface work function change on the Ag adatom gas concentration. A breakdown of the linear relationship is induced by the occurrence of the Ag adatom gas superstructure identified as Si(111) $\sqrt{21} \times \sqrt{21}$-Ag only observed below room temperature. We evidence below room temperature a confinement of the 2DEG on atomic terraces characterised by spatial inhomogeneities of the 2DEG-induced charge transfer along with temporal fluctuations. These variations mirror the Ag adatom gas concentration changes induced by the growth of 3D Ag islands and the occurrence of an Ehrlich-Schwoebel diffusion barrier of 155 ± 10 meV.

Owing to their fascinating properties, 2D electron gas systems (2DEG) have recently generated major breakthroughs in the field of condensed matter physics. For instance, the occurrence of a conductive 2D phase at the surface of oxides paves the way for the emerging field of functional oxide electronics[1]. 2D Dirac electron gas observed in graphene has been shown to surpass the long-standing 2DEG confined at the GaAs/AlGaAs interface to determine the Planck constant h using Quantum Hall resistance measurements[2]. 2DEG at metal/semiconductor interfaces have pushed the phenomenon of superconductivity downto its very 2D limit[3] and also shown intriguing electron localisation and metal-insulator transition[4]. Apart from homogeneous 2DEG systems, a growing need for nanostructured electron gas[5–7] is motivated by accessible breakthroughs in low dimensional electronics. Here, we focus on a well-documented 2DEG that is interestingly created by a charge transfer from a Ag 2D adatom gas (Ag-2DAG) to the so-called S_1 electronic surface state of the Si(111)$\sqrt{3} \times \sqrt{3}$-Ag reconstructed surface ($\sqrt{3}$-Ag)[8–12]. This charge transfer is responsible for an increase of the surface electrical conductance of 50% at room-temperature (RT) upon a Ag deposition as small as 0.03 ML on the $\sqrt{3}$-Ag surface[8].

In this paper, we evidence the unreported mutual confinement of a 2DEG and a 2DAG on atomic terraces as large as a few μm^2 in the temperature range 210–250 K that also evolves in time. More specifically we perform measurements of the Ag-2DAG concentration, c, and of the 2DEG-induced surface work function change using a single mesoscopic microscopy technique (low-energy electron microscopy, LEEM, see Methods for details). To validate our fine comprehension of the system, we first focus on the transition between the $\sqrt{3}$-Ag and the Si(111)$\sqrt{21} \times \sqrt{21}$-Ag surface reconstruction ($\sqrt{21}$-Ag) only observed below RT[13]. The demonstration of a linear dependence of the surface work function change on the Ag-2DAG concentration along with results from the literature confirm that the electron doping of the 2DEG is revealed by the work function changes. A breakdown of this linear relationship is observed above a critical Ag-2DAG concentration. Using a simple analytic model, we conclude that the breakdown results from the occurrence of the $\sqrt{21}$-Ag reconstruction. Below RT, we evidence the confinement of the 2DEG on atomic terraces upon Ag deposition and after the nucleation of 3D growing Ag islands. This regime is characterised by inhomogeneous spatial distributions and temporal fluctuations of the 2DEG charge transfer induced by the Ag-2DAG. The origin of the mutual 2DEG and Ag-2DAG confinement is

Aix Marseille Univ, CNRS, CINAM, Marseille, France. Correspondence and requests for materials should be addressed to F.C. (email: cheynis@cinam.univ-mrs.fr)

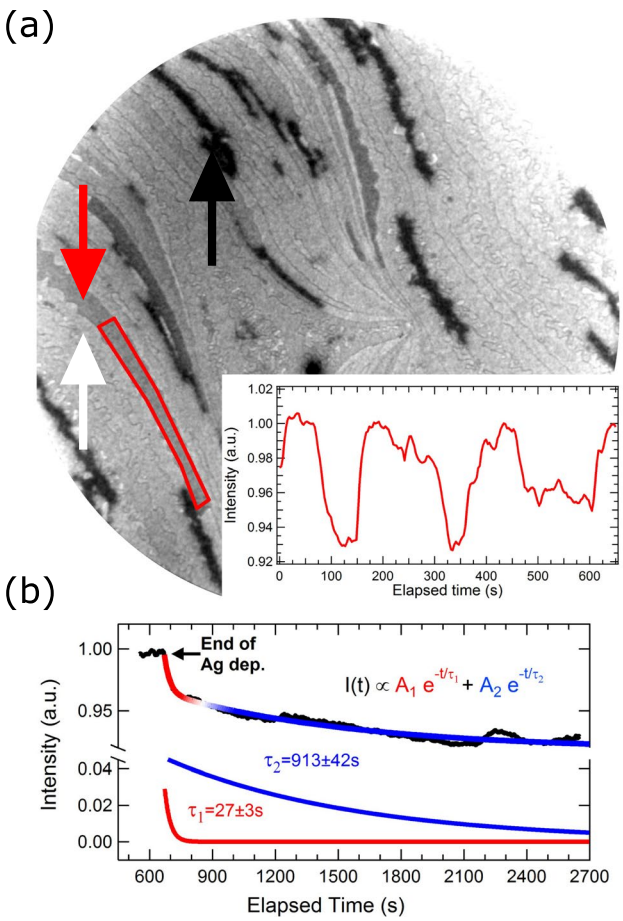

Figure 1. (**a**) LEEM image of a $\sqrt{3}$-Ag surface during a Ag deposition at 243 K after the nucleation of 3D Ag islands (black areas, see black arrow) showing intensity inhomogeneities as illustrated by the intensity difference between the two neighbouring terraces indicated by the white and red arrows (electron energy, $\varepsilon = 24$ eV, field-of-view, FOV = 15 μm). The inset illustrates the intensity time-evolution of the terrace highlighted in red in (**a**). (**b**) Time evolution of the LEEM image intensity averaged over the field-of-view (excluding 3D Ag islands) at the end of a Ag deposition at 220 K following the inhomogeneous regime ($\varepsilon = 24$ eV). τ_1 and τ_2 are the parameters determined by a double exponential fit of the intensity variation (red-to-blue curve). The two exponential fits (arbitrary vertical shift) are shown (red and blue curves).

interpreted as the result of the occurrence of an Ehrlich-Schwoebel diffusion barrier of 155 ± 10 meV below RT and of the interaction between the Ag-2DAG and growing 3D Ag islands.

Results

In Fig. 1, we qualitatively characterise the inhomogeneous regime. Figure 1(a) shows a LEEM image of a $\sqrt{3}$-Ag surface during a Ag deposition at 243 K. Apart from growing 3D Ag islands (black areas, see black arrow), the surface intensity is clearly inhomogeneous and varies from one atomic terrace to another (compare for instance the atomic terraces indicated by the red and white arrows, see also Supplementary Video S1 for real-time imaging). The inset evidences large intensity variations observed on an individual terrace as a function of time with quasi-stationary configurations of a few minutes and transitions occurring in only a few tens of seconds. Finally, for samples in the temperature range 210–250 K, the reflected intensity averaged over the imaged surface (excluding 3D Ag islands) remains inhomogeneous even in the absence of Ag deposition for times as long as 10–15 min. As shown in Fig. 1(b), the surface inhomogeneities relax in time unexpectedly with two well-identified exponential timescales, τ_1 and τ_2. The understanding of the inhomogeneous regime (including the two-component relaxation) constitutes the main goal of this report.

Let us first study the effect of the Ag deposition on the $\sqrt{3}$-Ag surface work function. As described in the Methods, the LEEM technique allows for the determination of the Ag adatom gas (Ag-2DAG) concentration on the $\sqrt{3}$-Ag surface and its induced work function change with respect to the initial $\sqrt{3}$-Ag surface. Figure S1 illustrates, for instance, that a deposition of 0.04 ML of Ag on the $\sqrt{3}$-Ag surface yields a shift of the Intensity-Electron beam energy curve, $I(\varepsilon)$, corresponding to a work function lowering of −0.23 eV. This confirms the electron donor role of the Ag adatoms to the $\sqrt{3}$-Ag surface state reported in refs 8, 10–12. Data in

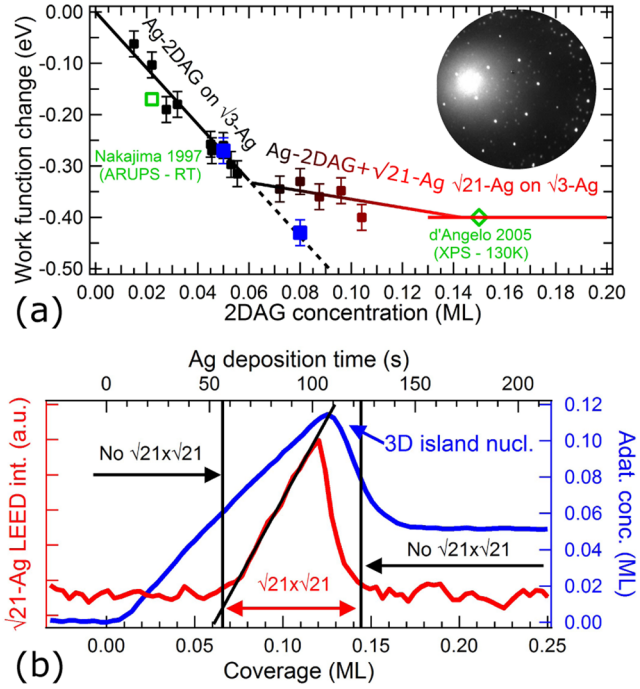

Figure 2. (**a**) Surface work function change with respect to the $\sqrt{3}$-Ag surface as a function of the Ag-2DAG concentration in the temperature range 210–470 K. The lines are data linear fits. Data from the literature are reported in green symbols (refs 8 and 16). The blue symbols show the work function change obtained in the inhomogeneous regime [see the insets in Fig. 3(b,d)]. The inset is a $\sqrt{21}$-Ag electron diffraction pattern. (**b**) Red curve: intensity real-time monitoring of the $\sqrt{21}$-Ag electron diffraction pattern upon Ag deposition at 228 K ($\varepsilon = 16.4$ eV). Blue curve: real-time monitoring of the Ag-2DAG concentration upon deposition at 210 K. The black line is a fit showing the linear dependence of the diffracted intensity of the $\sqrt{21}$-Ag reconstruction with respect to the Ag deposition.

Fig. 2(a) compile the characterisations of the Ag-2DAG concentration and the surface work function change for various samples in the temperature range 210–470 K.

For concentrations below 0.06 ML, the work function decreases linearly as the Ag-2DAG concentration increases, with a slope of $\Delta\phi_{\sqrt{3}} = -5.54 \pm 0.35$ eV/ML (black line). For comparison, we add in Fig. 2 the diminution of the S_1 surface state minimum of 0.17 eV measured by Y. Nakajima *et al.* in ref. 8 using Angle-Resolved UV-Photoemission Spectroscopy after a Ag-additional deposition of 0.022 ML. This value is in quantitative agreement with our data and confirms that the work function measurements characterise the 2DEG filling.

Above 0.06 ML, we evidence a breakdown of the initial linear relationship between the measured quantities [see the slope change between the black and the black-to-red lines in Fig. 2(a)]. These Ag-2DAG concentrations can only be obtained below RT (210–250 K). In this temperature range, a superstructure, identified by electron diffraction as $\sqrt{21}$-Ag[13], appears [see the inset of Fig. 2(a)]. This surface reconstruction is characteristic of a periodic arrangement of the Ag-2DAG on an preserved $\sqrt{3}$-Ag surface that only exists for a temperature-dependent finite coverage range[14,15]. The complete coverage of the surface by the $\sqrt{21}$-Ag reconstruction is expected at 0.143 ML (*i.e.* 1/7 of a ML and three Ag atoms per $\sqrt{21} \times \sqrt{21}$-unit cell).

To confirm the role of the $\sqrt{21}$-Ag reconstruction in the observed regime change, we have measured in real time the $\sqrt{21}$-Ag electron diffraction pattern (Fig. 2(b), red curve). We compare, under similar deposition temperature, its time-dependent intensity to a Ag-2DAG concentration monitoring obtained from the real-space imaging of the surface (Fig. 2(b), blue curve). We clearly evidence: *(i)* the $\sqrt{21}$-Ag electron diffraction pattern appears above 0.06 ML, *(ii)* its intensity increases linearly with the Ag deposition (black line) and *(iii)* its decay is triggered by the temperature-dependent 3D Ag island nucleation. From this, we can draw that the $\sqrt{21}$-Ag surface reconstruction requires a critical supersaturation before the nucleation of $\sqrt{21}$-Ag domains. The $\sqrt{21}$-Ag surface reconstruction coverage extends until 3D Ag islands nucleate. The maximum of the $\sqrt{21}$-Ag reconstruction coverage is determined by the temperature-dependent 3D Ag island nucleation. The complete coverage of the surface by the $\sqrt{21}$-Ag reconstruction at 0.143 ML needs deposition temperatures below 210 K to be reached. The observed decay of the $\sqrt{21}$-Ag reconstruction is caused by the growing 3D islands which consumes adatoms and destabilizes the $\sqrt{21}$-Ag dense reconstruction. Finally, our high concentration measurements [$\sim$0.1 ML, Fig. 2(a)] are compatible with a work function change of $\Delta\phi_{\sqrt{21}} = -0.4$ eV obtained by D'angelo *et al.* in ref. 16 using X-ray Photoemission Spectroscopy measurements at 130 K for a fully-covering $\sqrt{21}$-Ag reconstruction. The deviation from the initial linear dependence of the charge transfer with respect to the Ag-2DAG concentration and the

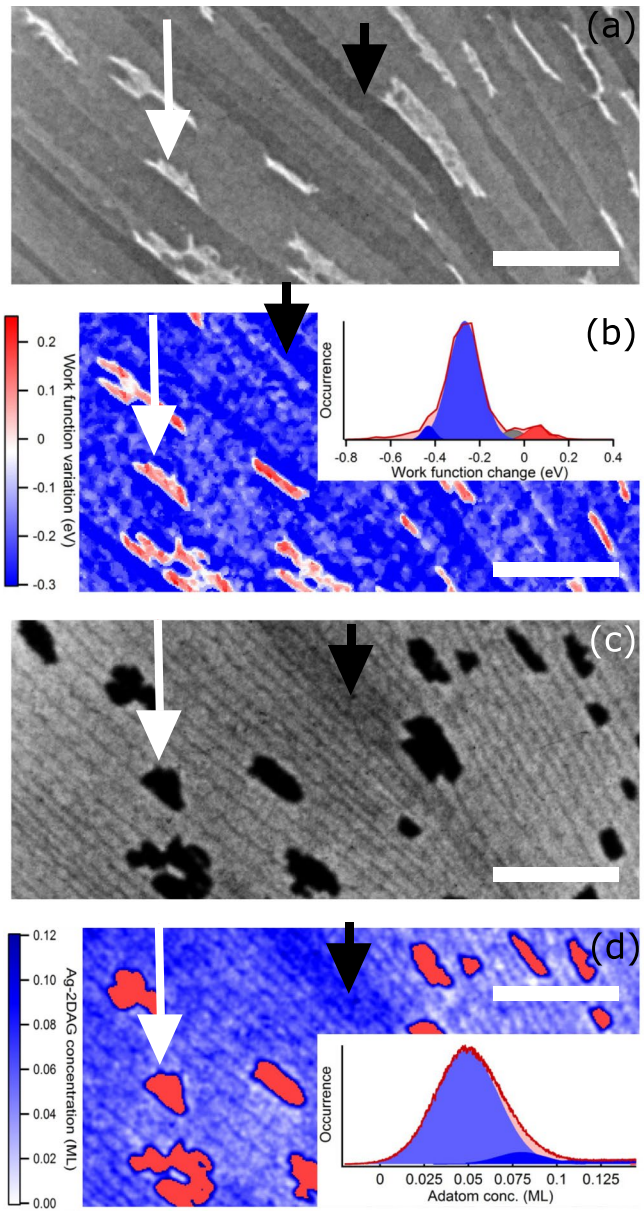

Figure 3. (**a**) Mirror Electron Microscopy image of a $\sqrt{3}$-Ag surface during a 2DAG-Ag deposition at 220 K after the nucleation of 3D island (white intensity) showing intensity inhomogeneities ($\varepsilon = 0$ eV). (**b**) 2D map of the surface work function change with respect to the $\sqrt{3}$-Ag surface obtained by reflectivity measurements (see Methods). The inset shows the histogram of the work function map. (**c**) LEEM image ($\varepsilon = 24$ eV) acquired 8 min before Fig. 3(a,b). (**d**) The 2D map of the Ag-2DAG concentration derived from image (**c**) (see Methods). The 3D Ag islands have been coloured in red in Fig. 3(d). The inset shows the histogram of the Ag adatom gas concentration. See the text for the arrow meaning. For all images, the scale bar is 2 μm.

saturation of the work function change at -0.4 eV are thus clearly attributed to the occurrence of the $\sqrt{21}$-Ag surface reconstruction. This is most probably due to the electronic localised state observed below RT in refs 11 and 12 which is possibly at the origin of the localised $\sqrt{21}$-Ag *D* state found in ref. 17.

To understand the deviation from the initial $\Delta\phi(c)$-linear relationship induced by the occurrence of the $\sqrt{21}$-Ag surface reconstruction, we propose a simple interpretation based on the mean work function change with respect to the initial $\sqrt{3}$-Ag surface. The work function change, $\Delta\phi$, is derived as the average between the contributions of both surface reconstructions (defined as $\Delta\phi_{\sqrt{3}}(c)$ and $\Delta\phi_{\sqrt{21}} = -0.4$ eV[16]) weighted by their respective area fraction. We assume that above the $\sqrt{21}$-Ag nucleation concentration, $c_{n,\sqrt{21}}$, additional Ag adatoms only contribute to the growth of the $\sqrt{21}$-Ag domains. In other words, a Ag-2DAG of concentration $c_{n,\sqrt{21}}$ coexist with a growing $\sqrt{21}$-Ag surface reconstruction. The $\sqrt{21}$-Ag reconstruction is indeed interpreted as a condensed configuration of the Ag-2DAG above a preserved $\sqrt{3}$-Ag surface[15]. In this model, $\Delta\phi$ reads:

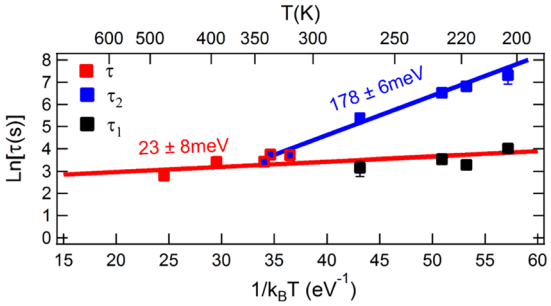

Figure 4. Arrhenius plot of the Ag-2DAG concentration relaxation time (τ) in the temperature range 210–470 K. Data obtained below RT require two characteristic times, τ_1 and τ_2, to fit satisfyingly the experimental data (see text for details).

$$\Delta\phi = \Delta\phi_{\sqrt{21}}\ \rho_{\sqrt{21}} + \Delta\phi_{\sqrt{3}}(c_{n,\sqrt{21}})\ (1 - \rho_{\sqrt{21}})$$

where $\rho_{\sqrt{21}} = (c - c_{n,\sqrt{21}})/(c_{m,\sqrt{21}} - c_{n,\sqrt{21}})$ is the area fraction covered by the $\sqrt{21}$-Ag reconstruction and $c_{m,\sqrt{21}} = 1/7 = 0.143$ ML[15,18] is the Ag-2DAG concentration for which the $\sqrt{21}$-Ag reconstruction reaches the maximum fraction area (*i.e.* $\rho_{\sqrt{21}}(c_{m,\sqrt{21}}) = 1$). The linear model is shown as a black-to-red line in Fig. 2(a) and fits the experimental data for $c_{n,\sqrt{21}} = 0.061 \pm 0.005$ ML. This threshold value for the onset of the $\sqrt{21}$-Ag surface reconstruction is in quantitative agreement with the occurrence of a $\sqrt{21} \times \sqrt{21}$ electron diffraction pattern at a value of $c \sim 0.06$ ML [Fig. 2(b)] which confirms the validity of our approach.

The onset of the inhomogeneous regime observed upon Ag deposition below RT follows the nucleation of the 3D Ag islands and the disappearance of the $\sqrt{21}$-Ag. Figure 3(a) and Supplementary Information show that sub-micron wide terraces can exhibit an intensity darker than the surface mean intensity over micron-scaled lengths (see black arrow) with time fluctuations. In-between transitions, the temporal evolution of the surface is sufficiently slow to allow for the determinations of the 2D work function map [Fig. 3(b)] and the Ag 2D concentration map [Fig. 3(d)]. Three distinct features can be identified in the 2D work function map and its histogram [see the inset of Fig. 3(b)]. Most of the surface exhibits a work function change with respect to a homogeneous $\sqrt{3}$-Ag surface of $\Delta\phi \simeq -0.27$ eV (light blue). 3D islands have a work function higher than the reference by typically 0.1–0.2 eV (white arrow). A $\sqrt{3}$-Ag work function value close to 4.55 eV[16,19] gives an absolute work function for the 3D islands in quantitative agreement with the value of 4.64 eV (4.72 eV resp.) reported for bulk Ag(100) (Ag(111) resp.) using photoelectric measurements[20]. Large terraces with a dark blue intensity (black arrow) are also observed and are characterized by $\Delta\phi \simeq -0.43$ eV.

These features can be better understood by looking at the Ag adatom gas concentration map and its histogram [see the inset of Fig. 3(d)]. The Ag-2DAG concentration and the 2D work function maps have been acquired with a time delay [typ. 8 min between Fig. 3(a–d)]. This results in slightly different spatial and size distributions of the Ag 3D islands. Also the time delay makes the one-to-one correspondence between the terrace work function changes and the local Ag-2DAG concentration difficult. However both 2D maps and their respective histograms exhibit convincing similarities. In particular, dark blue terraces observed in Fig. 3(b) and characterised by $\Delta\phi \simeq -0.43$ eV appear also as dark blue terraces in Fig. 3(c,d) with a Ag adatom concentration $c \simeq 0.08$ ML, as indicated by the black arrow. With the disappearance of the $\sqrt{21}$-Ag surface reconstruction, this data point ($c \sim 0.08$ ML, $\Delta\phi \sim -0.43$ eV) is unexpectedly in agreement with the initial $\Delta\varphi(c)$-linear relationship found for homogeneous surfaces [Fig. 2(b)]. When averaging over multiple atomic terraces, we derive a mean surface Ag-2DAG concentration of $c \simeq 0.05$ ML yielding a mean work function change of $\Delta\phi \sim -0.27$ eV which also perfectly matches the initial $\Delta\varphi(c)$-linear relationship. Data obtained in the inhomogeneous regime are reported in Fig. 2 as blue symbols. This demonstrates two results: (i) the observed temporal and spatial changes of the surface work function mirror the variations of the Ag-2DAG concentration (*i.e.* atomic terraces highly concentrated in Ag adatoms exhibit a high charge transfer). (ii) In the inhomogeneous regime, work function changes lower than −0.4 eV can be reached owing to the disappearance of the $\sqrt{21}$-Ag. The initial linear work function change/Ag adatom concentration relationship obtained on homogeneous surfaces is still locally verified in the inhomogeneous regime.

Discussion

In the following, we provide an explanation of the inhomogeneous regime based on experimental measurements that rely on the dependence of the charge transfer on the underlying Ag atomic processes (adsorption, diffusion, capture). In this regime, the Ag-2DAG concentration (resp. surface work function change) can locally increase (resp. decrease) by 60% in only ~30 s on atomic terraces as large as $\gtrsim 3\ \mu m^2$. Also it is worth highlighting that the inhomogeneous regime, observed upon Ag deposition below RT, follows the 3D island nucleation. This suggests that a non-equilibrium mass transfer between the growing 3D islands and the surrounding Ag-2DAG phase is at work.

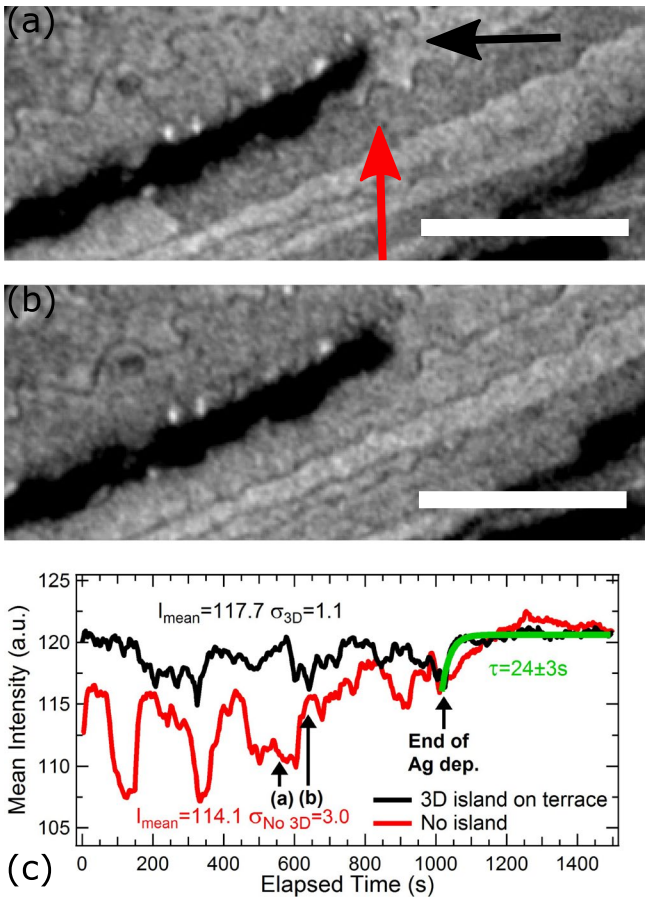

Figure 5. (**a,b**) Snapshots [from Fig. 1(a)] of the growth of a 3D island (black intensity) before (**a**) and after (**b**) it crosses the delimiting step with the terrace marked by the red arrow. Between (**a**) and (**b**), the adatom concentration of the terrace marked by the red arrow has decreased toward its stationary value ($c_{stat} \simeq 0.04$ ML). The scale bar is 1.5 μm and $\varepsilon = 24$ eV. (**c**) Intensity time-evolution of the atomic terraces indicated in (**a**) by red and black arrows. The timeline of the snapshots (**a**) and (**b**) is displayed.

In the data obtained at 220 K [Fig. 1(b)], the Ag-2DAG concentration relaxation after the end of the Ag deposition ($t = 670$ s) is not a simple exponential time-evolution as expected from nucleation theory[21]. Indeed, when adatoms are only captured by stable growing 3D islands, $\partial n_1/\partial t = -\sigma_x D n_x n_1$, where n_1, σ_x, D and n_x are respectively the adatom surface concentration, the adatom capture number, the adatom diffusion coefficient and the stable-island density. This gives $n_1(t) \sim e^{-t/\tau}$ with $\tau = 1/\sigma_x D n_x$ being the adatom relaxation time. In the inhomogeneous regime, two exponential functions with different timescales are required to obtain satisfying fits to the experimental data. This implies that additional activation barriers are involved below RT. One may think of the Ehrlich-Schwoebel barrier to cross atomic steps that would confine adatoms on terraces.

To confirm this hypothesis, we have characterised the Ag-2DAG concentration decay in the temperature range 210–470 K. In Fig. 4, we display the single characteristic time, τ, obtained for depositions above RT and the two timescales, τ_1 and τ_2, determined below RT as a function of the deposition temperature. The parameter τ_1 appears as the continuation of the characteristic time τ that characterises the capture of Ag adatoms by Ag 3D islands in the homogeneous regime. As such the short-timescale evolution of the Ag-2DAG concentration exhibits a relatively weak activation energy of 23 ± 8 meV over the explored temperature range (Fig. 4, red linear fit). On the other hand, τ_2 shows a more significant dependence on the temperature with an activation energy of 178 ± 6 meV (Fig. 4, blue linear fit). As τ_2 governs the relaxation dynamics below RT, the activation energy of the concentration relaxation time is increased by 155 ± 10 meV below RT. This increase compares remarkably well to the Ehrlich-Schwoebel barrier of Ag/Ag(111) self-diffusion of 150 ± 30 meV[22], 120 ± 20 meV[23] and 130 ± 40 eV[24] determined below or close to RT. In the low-temperature regime, high Ag adatom incorporation by attachment at atomic steps is likely due to a reduced surface diffusion. We can thus expect in this temperature regime a behaviour similar to the Ag/Ag(111) system. At higher temperatures, lateral strain relaxations at atomic steps are possible. This favours atom exchange mechanisms at steps that have been shown to be the preferred route over jump diffusion in the Ag/Ag(111) system[25] and in a very similar system Au/Si(111) $\sqrt{3} \times \sqrt{3}$-Au[26]. Although charge-dependent diffusion of Ag adatoms cannot be excluded[27], the above arguments strongly suggest that below RT, an additional Ehrlich-Schwoebel diffusion barrier limits the Ag-2DAG concentration equating between

terraces as well as the induced charge transfer and explains the long timescale behaviour of these quantities and specified by τ_2. This results in the confinement of adatoms on atomic terraces.

Besides the Ehrlich-Schwoebel diffusion barrier, the growth of 3D islands plays a major role in the occurrence of the inhomogeneous regime. Figure 5(a,b) are snapshots of Fig. 1(a) showing the growth of a 3D island (black intensity) on a terrace (black arrow) before and after it crosses a delimiting step and reaches a supersaturated neighbouring terrace (red arrow). The intensity of the terrace indicated by the red arrow clearly changes from dark grey to light grey suggesting a decrease of the Ag-2DAG concentration. This change is visible in the intensity time evolution of the terrace [Fig. 5(c)] at $t \simeq 600$s. The Ag-2DAG accumulated on the terrace indicated by the red arrow relaxes towards its stationary concentration ($c_{stat} \simeq 0.04$ ML) when the 3D island crosses the delimiting atomic step. Also, under Ag atom deposition, the intensity variation of a terrace occupied by a growing 3D island (Fig. 5(c), black curve) is much smaller than that of an unoccupied terrace (Fig. 5(c), red curve). High Ag-2DAG concentrations and charge transfer on atomic terraces exhibiting a 3D island cannot be reached owing to the adatom consumption by the growth of the 3D islands. Finally, atomic terraces hosting a growing 3D island show a rapid Ag-2DAG/charge transfer relaxation of ~30 s when the Ag flux is stopped (see for instance the black curve in Fig. 5(c) with a characteristic time of 24 ± 3 s) that compares well with the characteristic time τ_1. From these local measurements, we can infer that the short-time behaviour observed in the inhomogeneous regime and quantified by τ_1 corresponds to the capture of diffusing Ag adatoms by Ag 3D islands in their vicinity. This also confirms *a posteriori* that τ and τ_1 are the same quantity and clock the same phenomenon. The occurrence, below RT, of two distinct timescales (τ_1 and τ_2) resulting from the interplay between a Ag adatom gas with a hindered surface diffusion and a growing 3D phase convincingly explains the large variations of the Ag-2DAG concentration and 2DEG charge transfer.

Conclusion

In summary, we have monitored, upon Ag-deposition on a $\sqrt{3}$-Ag, the Ag-2DAG concentration and the corresponding surface work function change using LEEM. We have demonstrated that both quantities are linearly related and that the breakdown of the linear relationship is caused by the onset of the $\sqrt{21}$-Ag below RT. An unconventional regime showing inhomogeneous spatial distribution and temporal variations of both work function change and Ag-2DAG concentration is evidenced. The interaction between the growing 3D Ag islands and the Ag-2DAG plays a major role in the origin of this regime along with the occurrence of an Ehrlich-Schwoebel barrier of 155 ± 10 meV below RT. Inhomogeneous 2D electron gas in a quasi-permanent time configuration are likely to be obtained by quenching the system under study. These results are of high interest for the emerging field of low dimensional electronics.

Methods

Sample preparation. *n*- and *p*-doped Si(111) samples have been cleaned before loading into our ultra-high vacuum setup[28] for a complete characterization by Low-Energy Electron Microscopy (*LEEM III*, Elmitec GmbH). The sample temperature is determined using a type-C thermocouple spot-welded to the sample holder. We estimate that the typical measurement uncertainty is ±25 K. After a degas annealing (1–2 h at ~850K), samples have been flash heated at 1400–1500 K for a few tens of seconds and produced high quality 7×7 surface reconstruction (not shown). $\sqrt{3}$-Ag reconstructed surfaces are obtained by Ag deposition on a Si(111) surface below 750 K (typically 15 min for 1 ML-$\sqrt{3}$-Ag with 1 ML = 7.83×10^{14} atoms/cm^2[8]). 2DEG *per se* is obtained by an additional Ag deposition in the range 210–470 K under identical conditions.

LEEM and work function measurements. Low-Energy Electron Microscopy (LEEM) technique allows to determine the work function change of a surface (*e.g.* under deposition conditions) using Intensity-Electron beam energy, $I(\varepsilon)$, curves obtained from reflectivity measurements as a function of the incident electron beam energy averaged over areas exhibiting identical intensity[29–31].

At low incident electron beam energy, the sample work function is derived from the intersection of the two linear fits of the reflectivity curve obtained below and above the total reflection threshold. With this method, we estimate that the typical measurement uncertainty is ±25 meV. In Fig. S1, a $\sqrt{3} \times \sqrt{3}$-Ag surface shows at 220 K an electron beam injection threshold slightly above $\varepsilon = 0$ eV. Upon a Ag-2DAG deposition of 0.04 ML at 220 K a lowering of the electron beam injection threshold of $\Delta\phi = -0.23$ eV with respect to the $\sqrt{3} \times \sqrt{3}$-Ag surface is evidenced.

In both cases, the injection threshold also matches the condition $I/I_0 < 0.92$, where I_0 is the intensity backscattered from the surface in the total reflection regime. To determine unambiguously a surface work function using LEEM, a reference is needed to account for the work function of the electron gun. In the case of the Si(111)$\sqrt{3} \times \sqrt{3}$-Ag surface, previous studies by X-ray Photoelectron Spectroscopy have reported a work function value of 4.55 eV[16,19] which is very close to the value of the Si(111) 7×7 surface of 4.6 eV[32]. Instead of averaging the reflectivity curves over micron-sized areas, the work function can be also derived pixel-by-pixel for a given I(ε)-image stack using the condition $I/I_0 < 0.92$ as a criterion in the algorithm. To enhance the signal-to-noise ratio, a 3×3 average filter is employed. This procedure provides work function 2D maps[33,34] and paves the way for in-lab studies of surfaces showing inhomogeneously distributed work function.

LEEM & adatom concentration monitoring. Another major asset of the LEEM technique is that it enables to monitor the concentration of an adspecies in real-time[35–37]. The adspecies concentration, c, is obtained from the real-time monitoring of the reflectivity changes of a sample region as a function of the deposit, θ, at an adequate incident electron energy. This method is based on an approach developed for backscattered atomic

beams[38]. Applied to the LEEM electron beam, it reads $c = \frac{1}{\Sigma}\left(1 - \frac{I(\theta)}{I_0}\right)$, where Σ is the effective electron-adatom cross section and I_0 is the specular intensity with zero coverage. By comparing the LEEM $I(\varepsilon)$ curves of a sample before and after the deposition, a maximum of sensitivity to the deposited species can be determined. As shown in the the inset of Fig. S2, a significant reflectivity change induced by the Ag-2DAG deposition is observed for an incident electron energy of 24 eV. Using the slope at the origin in Fig. S2 to determine Σ (black line), the typical intensity variation upon Ag deposition on the Si(111)$\sqrt{3} \times \sqrt{3}$-Ag gives $c = 0.43 \times \left(1 - \frac{I(\theta)}{I_0}\right)$ and $\Sigma = 29 \pm 3$ Å^2, assuming a Ag-2DAG adsorption site density equal to that of the Si(111)$\sqrt{3} \times \sqrt{3}$-Ag (*i.e.* 7.83×10^{14} atoms/cm^2 [8]). This translate into a concentration measurement uncertainty of $\simeq$10%. The measured values of Σ are in quantitative agreement with previous study by LEEM on Ag/W(100)[35] and also close to the value of 47 Å^2 determined from He scattering measurements on Ag/Pd(100)[38].

The adspecies concentration monitoring allows to identify different Ag-deposition related regimes. First, the Ag-2DAG concentration increases linearly with time or equivalently with the amount of deposited Ag until it reaches a critical concentration (c_{nucl}) where 3D islands begin to grow on an unmodified $\sqrt{3}$-Ag surface as expected for a Stranski-Krastanov growth mode. After the 3D phase nucleation, the Ag-2DAG concentration decreases and reaches a stationary state (c_{stat}) where Ag adatom deposit, surface diffusion and consumption by the 3D growing phase are in a dynamical equilibrium. 2DAG concentration maps can also be determined. The $c\left(\frac{I}{I_0}\right)$ relationship is computed pixel-by-pixel (instead of micron-sized homogeneous areas) between an image obtained at 24 eV for a given coverage and a reference acquired before any deposition.

References

1. Santander-Syro, A. F. *et al.* Two-dimensional electron gas with universal subbands at the surface of $SrTiO_3$. *Nature* **469**, 189, doi:10.1038/nature09720 (2011).
2. Ribeiro-Palau, R. *et al.* Graphene surpasses GaAs/AlGaAs for the application of the quantum Hall effect in metrology. *Nature Nanotech.* **10**, 965, doi:10.1038/NNANO.2015.192 (2015).
3. Zhang, T. *et al.* Superconductivity in one-atomic-layer metal films grown on Si(111). *Nat Phys* **6**, 104, doi:10.1038/nphys1499 (2010).
4. Matsuda, I. *et al.* Electron-phonon interaction and localization of surface-state carriers in a metallic monolayer. *Phys. Rev. Lett.* **99**, 146805, doi:10.1103/PhysRevLett.99.146805 (2007).
5. Hermelin, S. *et al.* Electrons surfing on a sound wave as a platform for quantum optics with flying electrons. *Nature* **477**, 435, doi:10.1038/nature10416 (2011).
6. Palacio, I. *et al.* Atomic structure of epitaxial graphene sidewall nanoribbons: Flat graphene, miniribbons, and the confinement gap. *Nano Lett.* **15**, 182, doi:10.1021/nl503352v (2015).
7. Bhattacharya, A., Skinner, B., Khalsa, G. & Suslov, A. V. Spatially inhomogeneous electron state deep in the extreme quantum limit of strontium titanate. *Nat. Commun.* **7**, 12974, doi:10.1038/ncomms12974 (2016).
8. Nakajima, Y., Takeda, S., Nagao, T., Hasegawa, S. & Tong, X. Surface electrical conduction due to carrier doping into a surface-state band on Si(111) $-\sqrt{3}\times\sqrt{3}$-Ag. *Phys. Rev. B* **56**, 6782, doi:10.1103/PhysRevB.56.6782 (1997).
9. Aizawa, H. & Tsukada, M. First-principles study of Ag adatoms on the Si(111)$-\sqrt{3}\times\sqrt{3}-$Ag surface. *Phys. Rev. B* **59**, 10923, doi:10.1103/PhysRevB.59.10923 (1999).
10. Uhrberg, R. I. G., Zhang, H. M., Balasubramanian, T., Landemark, E. & Yeom, H. W. Photoelectron spectroscopy study of Ag/Si(111)$\sqrt{3}\times\sqrt{3}$ and the effect of additional Ag adatoms. *Phys. Rev. B* **65**, 081305, doi:10.1103/PhysRevB.65.081305 (2002).
11. Crain, J. N., Gallagher, M. C., McChesney, J. L., Bissen, M. & Himpsel, F. J. Doping of a surface band on Si(111)$\sqrt{3}\times\sqrt{3}$-Ag. *Phys. Rev. B* **72**, 045312, doi:10.1103/physrevb.72.045312 (2005).
12. Liu, C., Matsuda, I., Hobara, R. & Hasegawa, S. Interaction between adatom-induced localized states and a quasi-two-dimensional electron gas. *Phys. Rev. Lett.* **96**, 036803, doi:10.1103/PhysRevLett.96.036803 (2006).
13. Zhang, Z. H., Hasegawa, S. & Ino, S. Reconstruction and growth of ag on the Si(111)-$\sqrt{3}\times\sqrt{3}$-Ag surface at low temperature. *Phys. Rev. B* **52**, 10760, doi:10.1103/PhysRevB.52.10760 (1995).
14. Hasegawa, S., Tong, X., Takeda, S., Sato, N. & Nagao, T. Structures and electronic transport on silicon surfaces. *Prog. Surf. Sci.* **60**, 89, doi:10.1016/S0079-6816(99)00008-8 (1999).
15. Fukaya, Y., Kawasuso, A. & Ichimiya, A. Structural analysis of Si(111)-$\sqrt{21}\times\sqrt{21}$-Ag surface by reflection high-energy positron diffraction. *Surf. Sci.* **600**, 3141, doi:10.1016/j.susc.2006.05.045 (2006).
16. D'angelo, M. *et al.* Alkali metal-induced Si(111)$\sqrt{21}\times\sqrt{21}$ structure: The Na case. *Surf. Sci.* **590**, 162, doi:10.1016/j.susc.2005.06.031 (2005).
17. Tong, X. *et al.* Electronic structure of Ag-induced $\sqrt{3}\times\sqrt{3}$ and $\sqrt{21}\times\sqrt{21}$ superstructures on the si(111) surface studied by angle-resolved photoemission spectroscopy and scanning tunneling microscopy. *Phys. Rev. B* **64**, 205316, doi:10.1103/PhysRevB.64.205316 (2001).
18. Matsuda, I. & Hasegawa, S. Fermiology and transport in metallic monatomic layers on semiconductor surfaces. *J. Phys.: Condens. Matter* **19**, 355007, doi:10.1088/0953-8984/19/35/355007 (2007).
19. Hughes, G., Carty, D., McDonald, O. & Cafolla, A. Synchrotron radiation photoemission studies of the pentacene-Ag/Si(111)$\sqrt{3}\times\sqrt{3}$. *Surf. Sci.* **580**, 167, doi:10.1016/j.susc.2005.02.019 (2005).
20. Dweydari, A. W. & Mee, C. H. B. Work function measurements on (100) and (110) surfaces of silver. *Phys. Status Solidi (a)* **27**, 223, doi:10.1002/pssa.2210270126 (1975).
21. Venables, J. A., Spiller, G. D. T. & Hanbücken, M. Nucleation and growth of thin films. *Rep. Prog. Phys.* **47**, 399, doi:10.1088/0034-4885/47/4/002 (1984).
22. Vrijmoeth, J., van der Vegt, H. A., Meyer, J. A., Vlieg, E. & Behm, R. J. Surfactant-induced layer-by-layer growth of Ag on Ag(111): Origins and side effects. *Phys. Rev. Lett.* **72**, 3843, doi:10.1103/PhysRevLett.72.3843 (1994).
23. Bromann, K., Brune, H., Röder, H. & Kern, K. Interlayer mass transport in homoepitaxial and heteroepitaxial metal growth. *Phys. Rev. Lett.* **75**, 677, doi:10.1103/PhysRevLett.75.677 (1995).
24. Morgenstern, K., Rosenfeld, G., Lægsgaard, E., Besenbacher, F. & Comsa, G. Measurement of energies controlling ripening and annealing on metal surfaces. *Phys. Rev. Lett.* **80**, 556, doi:10.1103/PhysRevLett.80.556 (1998).
25. Ferrando, R. & Tréglia, G. Step-descent mechanisms on Ag and Au(111). *Surf. Sci.* **377**, 843, doi:10.1016/S0039-6028(96)01515-4 (1997).
26. Curiotto, S., Leroy, F., Cheynis, F. & Müller, P. Surface diffusion of Au on $\sqrt{3}\times\sqrt{3}$ Si(111)-Au studied by nucleation-rate and Ostwald-ripening analysis. *Surf. Sci.* **647**, 8, doi:10.1016/j.susc.2015.11.015 (2016).
27. Repp, J. *et al.* Charge-state-dependent diffusion of individual gold adatoms on ionic thin NaCl films. *Phys. Rev. Lett.* **117**, 146102, doi:10.1103/PhysRevLett.117.146102 (2016).

28. Cheynis, F. *et al*. Combining low-energy electron microscopy and scanning probe microscopy techniques for surface science: development of a novel sample-holder. *Rev. Sci. Instrum.* **85**, 043705, doi:10.1063/1.4871437 (2014).
29. Babout, M., Guittard, C., Guivarch, M., Pantel, R. & Bujor, M. Mirror electron microscopy applied to the continuous local measurement of work-function variations. *J. Phys. D: Appl. Phys.* **13**, 1161, doi:10.1088/0022-3727/13/7/011 (1980).
30. Murata, Y. *et al*. Growth structure and work function of bilayer graphene on Pd(111). *Phys. Rev. B* **85**, 205443, doi:10.1103/physrevb.85.205443 (2012).
31. Jin, X. *et al*. Low energy electron microscopy and auger electron spectroscopy studies of Cs-O activation layer on p-type GaAs photocathode. *J. Appl. Phys.* **116**, 174509, doi:10.1063/1.4901201 (2014).
32. Mönch, W. *Semiconductor Surfaces and Interfaces, vol. 26 of Springer Series in Surface Sciences* (Springer Berlin Heidelberg, 2001).
33. Rault, J. E. *et al*. Thickness-dependent polarization of strained $BiFeO_3$ films with constant tetragonality. *Phys. Rev. Lett.* **109**, 267601, doi:10.1103/PhysRevLett.109.267601 (2012).
34. Kautz, J., Jobst, J., Sorger, C., Tromp, R. M. & Weber, S. J. H. B.and van der Molen. Low-energy electron potentiometry: Contactless imaging of charge transport on the nanoscale. *Sci. Rep.* **5**, 13604, doi:10.1038/srep13604 (2015).
35. de la Figuera, J., Bartelt, N. & McCarty, K. Electron reflectivity measurements of Ag adatom concentrations on W(110). *Surf. Sci.* **600**, 4062, doi:10.1016/j.susc.2006.02.069 (2006).
36. Loginova, E., Bartelt, N. C., Feibelman, P. J. & McCarty, K. F. Factors influencing graphene growth on metal surfaces. *New J. Phys.* **11**, 063046, doi:10.1088/1367-2630/11/6/063046 (2009).
37. Schwarz, D., van Gastel, R., Zandvliet, H. J. W. & Poelsema, B. Phase transformations of 4,4′-biphenyldicarboxylic acid on Cu(001). *Phys. Rev. B* **85**, 235419, doi:10.1103/PhysRevB.85.235419 (2012).
38. Farias, D. & Rieder, K.-H. Atomic beam diffraction from solid surfaces. *Rep. Prog. Phys.* **61**, 1575, doi:10.1088/0034-4885/61/12/001 (1998).

Author Contributions

F.C. conceived and carried out the experiments. F.C. analysed the results and all authors took part in discussing the results. F.C. wrote the manuscript text with input from all the authors. All authors reviewed the manuscript.

Additional Information

Supplementary information accompanies this paper at doi:10.1038/s41598-017-10300-6

Competing Interests: The authors declare that they have no competing interests.

Publisher's note: Springer Nature remains neutral with regard to jurisdictional claims in published maps and institutional affiliations.